Prevalence of Anisotropic Shell Growth in Rare Earth Core–Shell Upconversion Nanocrystals

Chao Zhang and Jim Yang Lee*

Department of Chemical and Biomolecular Engineering, National University of Singapore, 10 Kent Ridge Crescent, Singapore 119260, Republic of Singapore

ABSTRACT Through a series of carefully executed experiments, we discovered the prevalence of anisotropic shell growth in many upconversion $NaREF_4$ systems caused by a combination of factors: selective adsorption of ligands on the core surface due to the core crystal structure, ligand etching, and the lattice mismatch between core and shell components. This could lead to incomplete shell formation in core–shell nanocrystals under certain conditions. Shell growth is always faster in the *a* and *b* crystallographic directions than in the *c* direction. In the case of a larger lattice mismatch between the core and shell, shell growth only occurs in the *a* and *b* directions resulting in an oblong core–shell structure. These findings are useful for rationalizing shell-dependent emission properties, understanding the emission mechanisms in complex core–shell nanostructures, and for creating accurate models of core–shell designs for multifunctionality and optimal performance in applications.

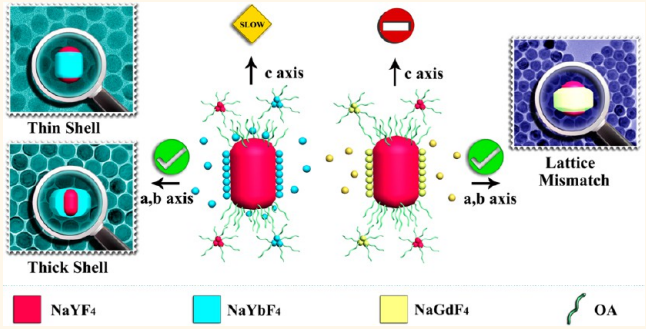

KEYWORDS: upconversion nanocrystals · core–shell · anisotropy · rare earth · photoluminescence

There has been strong interest since the past decade to use rare earth (RE) upconversion (UC) nanocrystals (NCs) for bioimaging, magnetic resonance imaging (MRI) and photodynamic therapy (PDT). Excellent luminescent properties enabling high contrast imaging and low cell and tissue damages are the notable advantages of RE-based UC NCs.[1−20] Currently, Yb^{3+} and Tm^{3+} (or Er^{3+}) co-doped hexagonal $NaREF_4$ UC NCs are the most extensively researched RE-based UC NCs for bioimaging. For the continuing development of RE-based UC NCs into multimode imaging agents, further improvement of their luminescence performance and increase in color variety are required, and core–shell (CS) construction is the commonest means.[1,18−26] The expected outcomes could only be delivered if the core and shell can be fabricated exactly according to the design with high crystallinity and precise composition control. Moreover, the current understanding of the emission mechanisms in complex UC CS systems (having two and more emitters) is mostly predicated upon some ideal core–shell features, *e.g.*, complete shell enclosure and uniform shell thickness. If these assumptions are not borne out by shell growth under practical conditions, the theory may have to be revised suitably.

There are still many unanswered questions in current research: *e.g.*, how does a shell grow on a hexagonal $NaREF_4$ core? What geometric model should be used for calculating the amount of shell precursor to grow to a given thickness? Why is luminescence not effectively enhanced by a thin shell?[4,24] Does the lattice mismatch between core and shell affect shell growth? These questions have not been answered because of the difficulty in synthesizing high quality CS NCs thereby causing uncertainties in the measurement of shell thickness in different directions. The nucleation of the "shell" as a separate phase, and the disorder in the CS NC deposition on the copper grid for TEM examination, could also result in different "thickness" measurements and erroneous conclusions. Besides, most frequently reported UC CSs contain quasi-spherical cores with shells of only a

* Address correspondence to cheleejy@nus.edu.sg.

Received for review February 22, 2013 and accepted April 9, 2013.

Published online April 09, 2013
10.1021/nn4009214

few nanometers. The accurate measurement of shell thickness in different directions is difficult in this case. Often the CS structure is inferred from changes in the size of the core in a growth solution, assuming uniform shell growth on the core. This assumption is not valid except for an amorphous shell. Furthermore, anisotropy in the core NC, dissimilar surface energy of different exposed faces, etching by ligands, and the lattice mismatch between core and shell components can also give rise to anisotropy in an epitaxially grown shell. Unfortunately, shell anisotropy was largely overlooked in many of the previous studies on CS UC NCs. Although nonuniform shell growth had been observed in some of these studies, it was often attributed to some inadequacies in the synthetic procedures and as such an annoyance not worthy of further investigations.[24,27] Anisotropic shell growth can only be demonstrated in systems with certainty under very stringent control of the synthetic procedures where the more trivial causes for shell nonuniformities are absent. The purpose of this study is to demonstrate the universality of anisotropic shell growth and to show that complete shell enclosure is not an experimental certainty.

Shell growth was studied here by fine-tuning the shell thickness of a number of CS and core−shell−shell (CSS) nanostructures (NSs): $NaYF_4$:Yb^{3+}, Er^{3+}@$NaYbF_4$; $NaYF_4$:Yb^{3+}, Er^{3+}@$NaYbF_4$:Tm^{3+}; $NaYF_4$:Yb^{3+}, Er^{3+}@$NaGdF_4$; $NaYF_4$:Yb^{3+}, Er^{3+}@ $NaGdF_4$:Eu^{3+}; $NaYF_4$:Yb^{3+}, Er^{3+}@$NaYbF_4$@$NaGdF_4$. These NCs with different types of core and shell components were produced by modifying a reference method (see Supporting Information). CS NCs with both thin and thick shells were prepared to contrast the comparison. By following the evolution of these NCs carefully, it was concluded that shell growth is highly anisotropic in the oleic acid synthesis system: the shell tends to grow from the six lateral faces than along the *c* axis, especially when the shell is thin. This preferential growth is independent of the core morphology, shell composition ($NaYbF_4$ or $NaGdF_4$), and reaction temperature (from 280 to 320 °C). In addition, the lattice mismatch between the core and shell also exerts significant influence on the shell growth directions. Oblong CS NCs with incomplete shell enclosure are formed if the lattice mismatch is sufficiently large.

RESULTS AND DISCUSSION

A slightly modified reference method was used for the syntheses of core NCs, CS and CSS NSs. Different from the reference method which uses thermal decomposition at high temperature and direct cooling thereafter, an additional ripening process at 280 °C was introduced after thermal decomposition at 320 °C to improve the uniformity of the core NCs. In addition, a slightly lower shell growth temperature (280 °C) was also used to produce high quality CSs and CSSs and to minimize etching by ligands. It was found that oleic acid etching occurred in the synthesis system, although this was not mentioned in previous work. Figure S1 shows the changes in the size and morphology of the core (short hexagonal prismatic NCs) before and after redispersion in the oleic acid -1-octadecene reaction system and reheating at 300 °C for 20 min. The treatment transformed the short rod-like hexagonal NCs into ellipsoidal nanoparticles (NPs). In addition, some small fragments were also found among the etched NCs. Besides the morphological changes, there was also a slight decrease in the average length of the NCs in the ⟨0001⟩ direction. This indicates that oleic acid etching of the NCs is orientation selective and is faster in the *c* axis than in the lateral directions. The observed selectivity in ligand etching is not surprising since ligand adsorption on NCs is known to be highly selective in most cases. Etching was minimized in the modified reference synthesis method but was not completely eliminated. Consequently, ligand etching could still occurr during epitaxial shell growth. The competition between ligand etching and shell deposition was expected to be more acute when the shell was thin.

The study of shell growth behavior in CS UC NCs through accurate measurements of the increase in shell thickness in all directions began with the preparation of uniform hexagonal rod-like $NaYF_4$:20% Yb^{3+}, 2% Er^{3+} NCs with aspect ratio (AR) of ∼1.5 (See TEM images in Figure 1a−d. The low-magnification TEM images in Figure S2 show the uniformity of the NCs by sampling over a large area). The growth of $NaYbF_4$ shells was studied first as an example of closely matched core and shell components (Y^{3+} and Yb^{3+} are similar in size and $NaYF_4$ and $NaYbF_4$ have closely matched lattice parameters). After the growth of a thin shell to thickness of 1 and 2 nm (Figure 2a,f,k, and b,g,l), the NCs became ellipsoidal in shape. The morphological change was caused by ligand etching under the condition of a low shell precursor concentration (better uniformity of CS NSs was obtained under this condition). Careful examination of these CS NCs revealed practically no shell growth in the ⟨0001⟩ direction when the shell on the lateral faces was 1 nm thick or lower. Shell growth along the *c* axis, however, did occur to a thickness of 0.35 nm, when the shell thickness on the lateral faces was increased to 2 nm. The presence of Yb^{3+} in both core and shell regions and the thinness of the shell made it difficult to analyze anisotropic shell growth in thin CS NCs by energy dispersive spectroscopy (EDS). XPS, which has a sampling depth of only several nanometers, was used instead. In the XPS spectra of core NCs in Figures S3 and S4, the Y^{3+} 3d and 3p peaks are more intense than the Yb^{3+} 4d peak. After the deposition of a 2 nm $NaYbF_4$:1% Tm^{3+} shell, the intensity of Yb^{3+} 4d peak was elevated to the level of the Y^{3+} 3d peak. Further shell growth to 10 nm

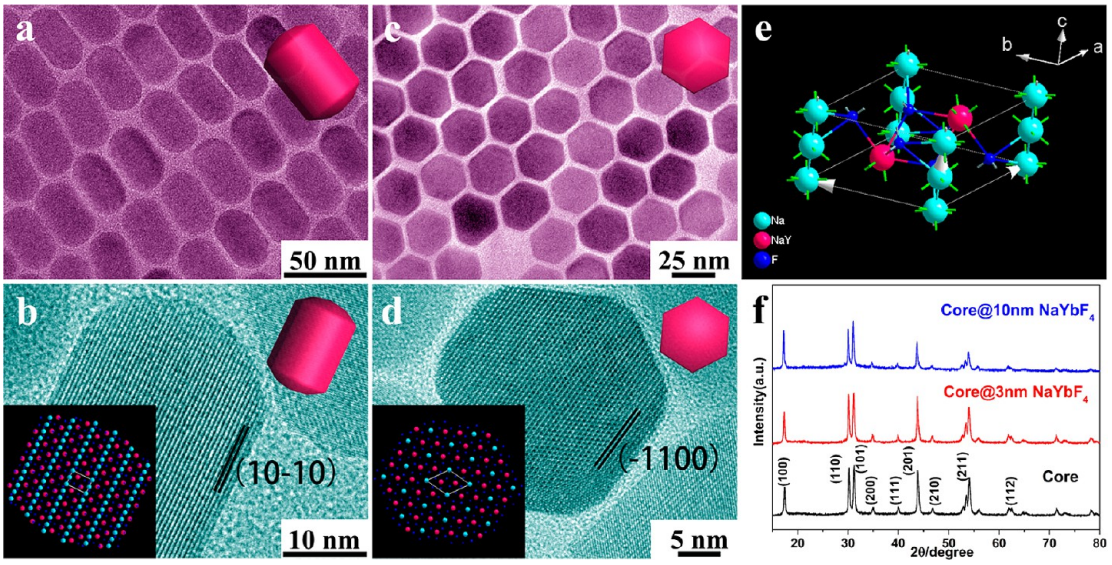

Figure 1. (a) TEM images of self-assembled (on a TEM Cu grid) rod-like hexagonal prismatic $NaYF_4$:20% Yb^{3+}, 2% Er^{3+} NCs with aspect ratio of 1.5 standing on their lateral faces. (b) HRTEM images of rod-like NCs in the ⟨0100⟩ direction; the inset is a schematic of their atomic structure. (c) TEM images of self-assembled (on a TEM Cu grid) rod-like hexagonal prismatic $NaYF_4$:20% Yb^{3+}, 2% Er^{3+} NCs with aspect ratio of 1.5 standing on their (0001) faces. (d) HRTEM images of rod-like NCs in the ⟨0001⟩ direction; the inset is a schematic of their atomic structure. (e) Unit cell of $NaYF_4$. (f) XRD patterns of $NaYF_4$:20% Yb^{3+}, 2% Er^{3+} NCs (black), $NaYF_4$:20% Yb^{3+}, 2% Er^{3+} NCs@3 nm $NaYbF_4$ (red), and $NaYF_4$:20% Yb^{3+}, 2% Er^{3+} NCs@10 nm $NaYbF_4$ (blue).

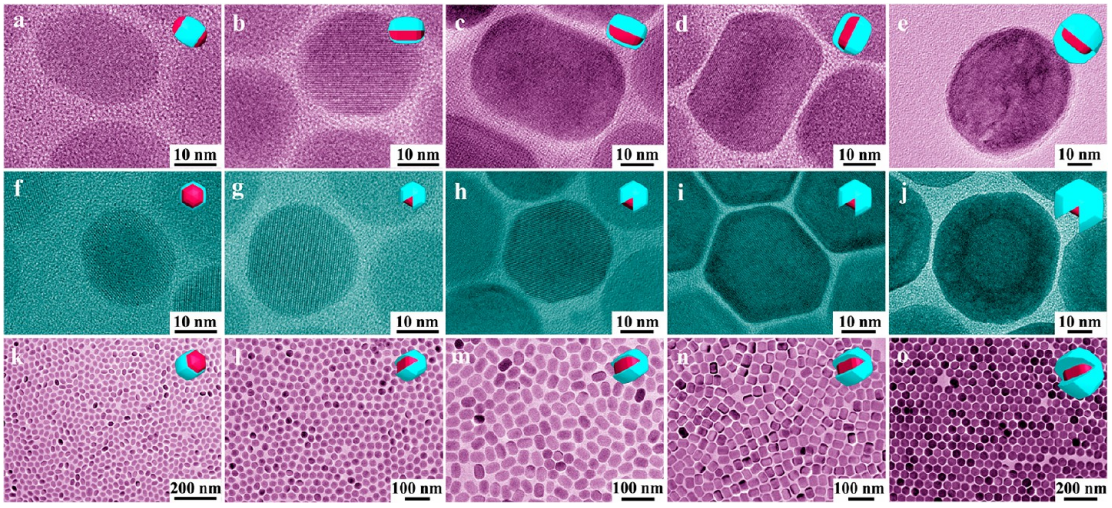

Figure 2. TEM images of rod-like hexagonal prismatic $NaYF_4$:20% Yb^{3+}, 2% Er^{3+}@$NaYbF_4$ with different shell's thickness: (a, f, and k) 1 nm; (b, g, and l) 2 nm; (c, h, and m) 3 nm; (d, i, and n) 4 nm; (e, j, and o) 12 nm. (a–e) Views from the ⟨0100⟩ direction. (f–j) Views from the ⟨0001⟩ direction. (k–o) TEM images of CS NSs when sampled over a large area of the Cu TEM grid.

witnessed the diminishment of the Y^{3+} 3d and 3p signals to almost the background level. These results confirmed the formation of CS NSs. Larger NCs were also prepared since anisotropic shell growth should be easier to detect in CS NCs with larger cores. These NCs could also provide information on the dependency of anisotropic shell growth on core size (~31.7 (length, along *c* axis) × 21.5 nm (diameter) and ~43 × 27.5 nm). Figure 2c–e, 2h–j, and 2m–o are the TEM images of $NaYF_4$:20% Yb^{3+}, 2% Er^{3+}@$NaYbF_4$ CS NSs with 3, 4, and 12 nm shells, respectively (see Table S1 for more details of these NCs). Anisotropic shell growth in this case could be detected by TEM as morphological changes between the top and side views of NCs with different shell thicknesses. The growth rates of the six lateral faces were higher than that in the ⟨0001⟩ direction. Anisotropy was also confirmed by the EDS analysis of $NaYF_4$:20% Yb^{3+}, 2% Er^{3+}@$NaYbF_4$ CS NSs with 4 and 12 nm thick shells standing on their (0001) face and lateral faces (Figure S5 and Figure 3, respectively). The spatial relationship between the core and shell obtained by comparing the element maps of Y^{3+} and Yb^{3+} in the ⟨0001⟩ direction and normal to the lateral faces (Figure 3b,c,e,g) also implied the higher

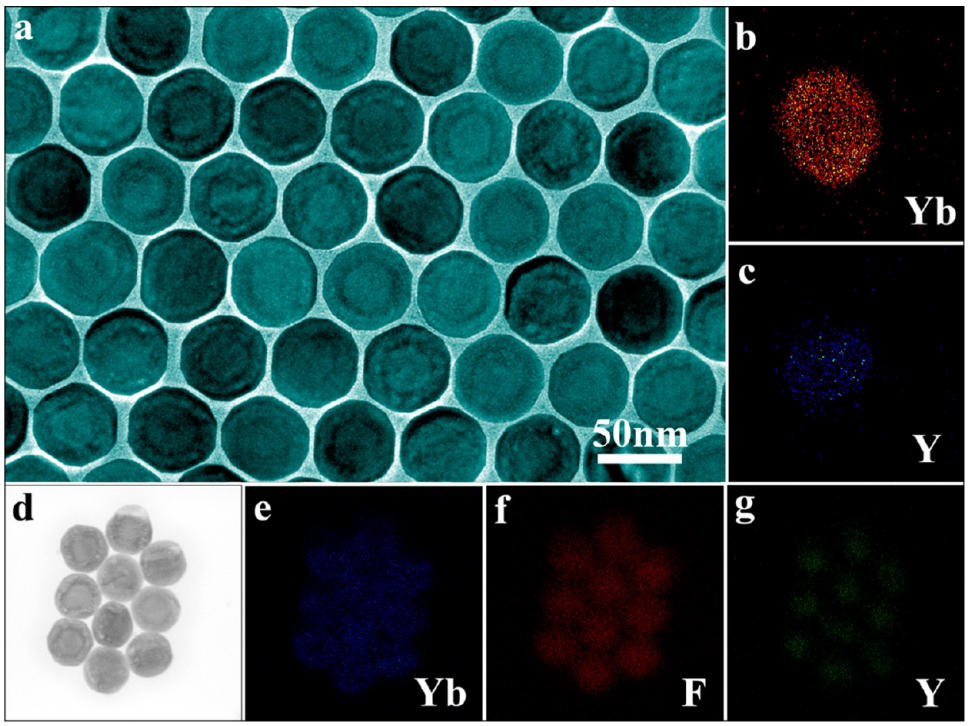

Figure 3. (a) TEM image of $NaYF_4$:20% Yb^{3+}, 2% Er^{3+}@12 nm $NaYbF_4$. (b and c) The component element maps (colored) from a CS NS standing on its lateral face; orange and blue indicate ytterbium and yttrium, respectively. (d) STEM image of the CS NSs. (e−g) The component maps (colored) from CS NSs standing on (0001) faces, blue, orange, and green indicate ytterbium, fluoride and yttrium, respectively.

growth rates of the lateral faces. XRD provided yet another evidence for the anisotropic growth of the CS structure. The XRD patterns of the CS NCs (Figure 1f, all of them are indexable to JCPDF: 28-1192) are all consistent with the anisotropy in shell thickness: increase in the thickness of the epitaxially grown shell also increased the relative intensity of the (100) diffraction peaks. This is because anisotropic shell growth resulted in a higher number of atomic layers in the lateral directions, as well as more CSs standing on their (0001) faces. It can therefore be concluded from these observations that the growth of $NaYbF_4$ on $NaYF_4$: Yb^{3+}, Er^{3+} is highly anisotropic.

For the study of the effects of morphology on anisotropic shell growth, small quasi-spherical NPs (~20 nm in length, Figure 4a) and large hexagonal prisms (~72 nm in diameter and 66 nm in length, Figure 4f) were used as the cores for the growth of $NaYbF_4$ shells. These NCs, together with the rod-like NCs, constitute the three most common morphologies that can be formed in an oleic acid synthesis system. Anisotropic shell growth also occurred in both cases, as shown in the TEM images in Figure 4 (more details in Table. S1 and Figure S6). For the growth to a 5 nm $NaYbF_4$ shell on quasi-spherical cores, higher growth rates (more than 3 times of that along the *c* axis. The growth rates were estimated by counting the number of atomic layers in the shells) were detected in the $\langle 1010 \rangle$, $\langle 1100 \rangle$, $\rangle 01\bar{1}0 \rangle$, $\langle 10\bar{1}0 \rangle$, $\langle 1\bar{1}00 \rangle$, and $\langle 0110 \rangle$ directions. The anisotropic shell growth became more conspicuous with the increase in shell thickness. Preferential shell growth in specific directions also prevailed in CS NSs with large prismatic cores, as shown in Figure 4f−i. The increasing diffraction intensities of the (100) planes relative to the other planes again correlated well with the shell thickness on the large hexagonal prisms from 5 to 20 and 25 nm (as shown in the XRD patterns in Figure S7), demonstrating once more the higher growth rates in the lateral directions. The observed anisotropic growth could not be eliminated by reaction temperature adjustments within the controlled range of experimental conditions.

$NaYF_4$ based UC NCs with $NaGdF_4$ shells are currently the most studied UC CS NS because of their ability to support dual model imaging and tuning of upconversion.[1,4,28] A good understanding of the anisotropic epitaxial growth in these CS NCs is particularly important for Gd^{3+} based MRI and migration-mediated upconversion. The emission mechanisms in complex CS NS are very different in the presence of absence of a complete shell. For MRI applications a thick shell is not helpful. These considerations underline the importance of an accurate geometric model for the precision fabrication of these NCs. We observed that the deposition of a $NaGdF_4$ shell on $NaYF_4$:20% Yb^{3+}, 2% Er^{3+} resulted in nearly no growth in the $\langle 0001 \rangle$ direction. Figure 5a,d, and b,e are the TEM

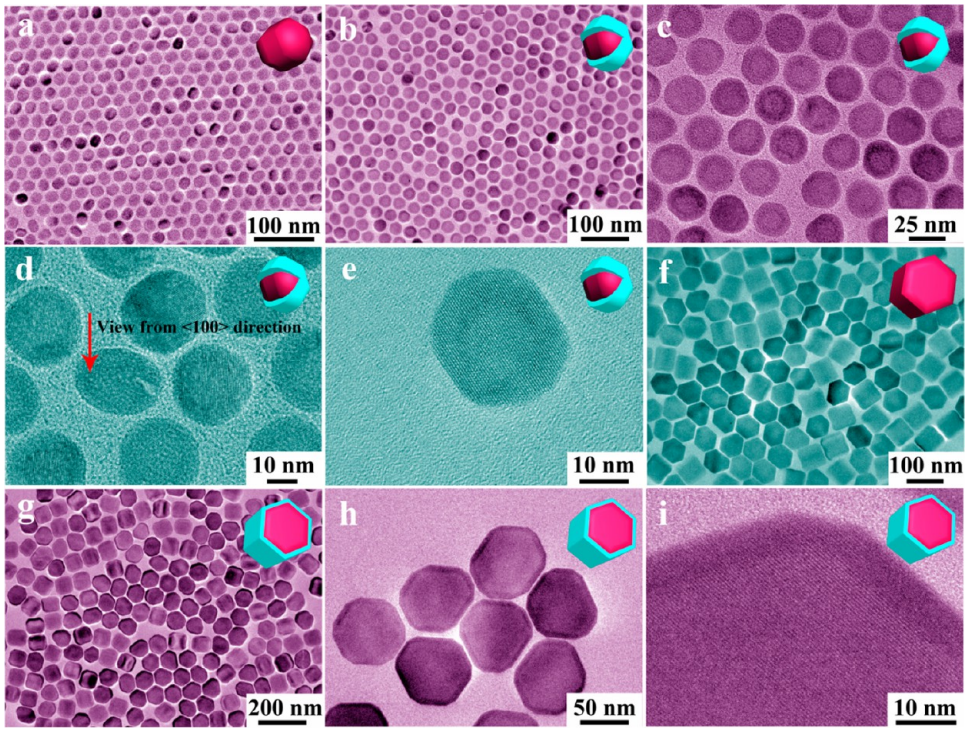

Figure 4. TEM images of 20 nm $NaYF_4$:20% Yb^{3+}, 2% Er^{3+} quasi-spherical NCs and large hexagonal prisms and the CS NSs with 5 nm $NaYbF_4$ shell for each: (a) quasi-spherical NCs; (b−e) quasi-spherical NCs with a 5 nm $NaYbF_4$ shell; (f) large hexagonal prisms; (g−i) large hexagonal prisms with a 5 nm $NaYbF_4$ shell.

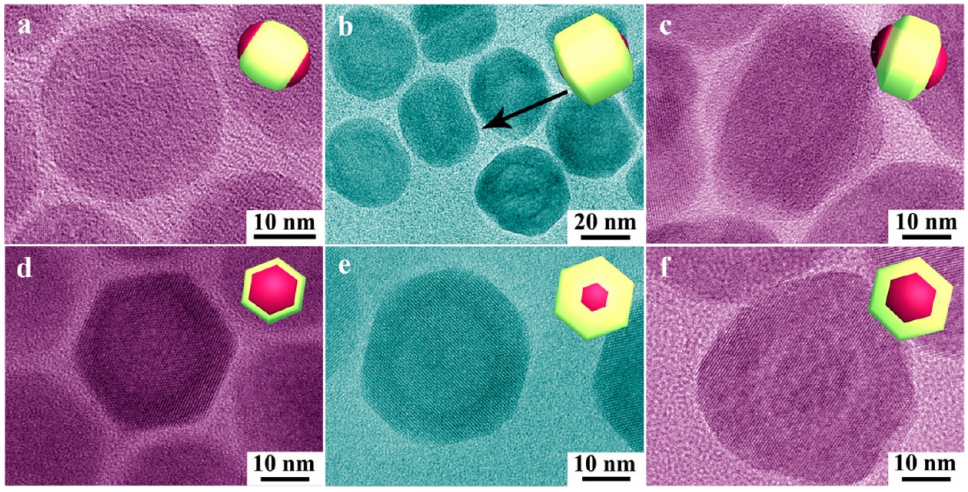

Figure 5. TEM images of $NaYF_4$:20% Yb^{3+}, 2% Er^{3+} NCs with different $NaGdF_4$ shells: (a and d) 4 nm $NaGdF_4$ shell; (b and e) 8 nm $NaGdF_4$ shell; (c and f) 10 nm $NaGdF_4$:10% Eu^{3+} shell. (a−c) Views from the ⟨0100⟩ direction. (d−f) Views from the ⟨0001⟩ direction.

images of the CS NCs with 4 and 8 nm-thick $NaGdF_4$ shells, respectively (low magnification TEM images showing the same CSs sampled over a larger area are given in Figure S8). The CS structure of these NCs was confirmed by the XRD and EDS data in Figures S9 and S10. Interestingly, unlike the $NaYbF_4$ shell, $NaGdF_4$ only grew on the side faces regardless of the shell thickness. This extreme anisotropic growth was caused by the relatively large lattice mismatch (2.6%) between the (0001) planes of the $NaGdF_4$ shell and the $NaYF_4$ core, as well as the different ionic radii of Y^{3+} and Gd^{3+} (Table S2). For small lattice structure and ionic radius mismatches, initial shell growth will follow the lattice of the core. The shell gradually relaxes into its own lattice structure with the buildup in shell thickness. The lattice strain at the interface causes significant stresses in the core and the shell. The shell then grows in a way to share as few common interfacial ions along the *c* axis as possible.[29,30] This hypothesis was tested by doping the $NaGdF_4$ shell with Eu^{3+}, an even larger ion (Figure 5c,f,

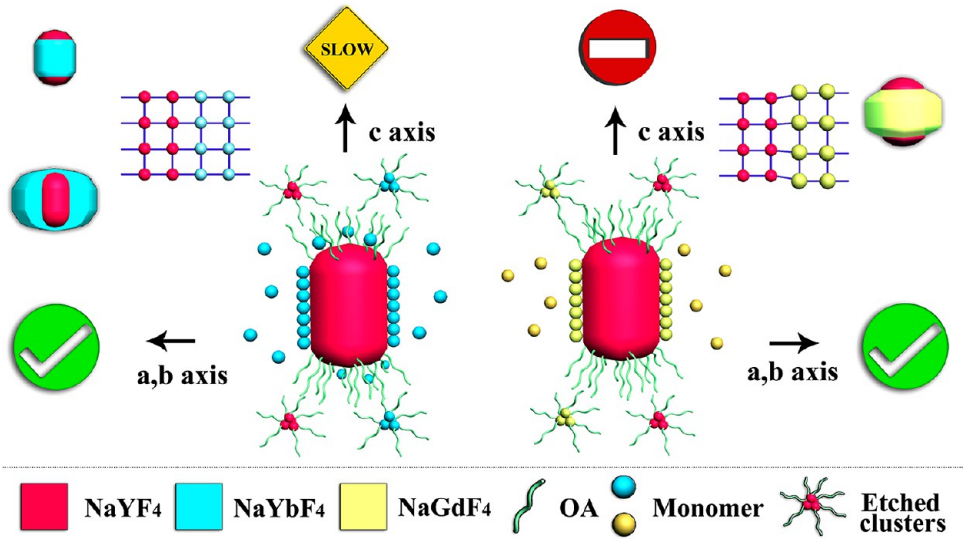

Figure 6. Schematic of anisotropic shell growth in UC CS NSs.

Figure S8, and Table S2), to increase the interfacial strain. The shell in this case shared fewer atoms with the core along the "c" axis. There was more deformation in the shell as evinced by the appearance of some partially twinned structures. Not limited to the CS NSs, CSS NCs of this UC system also exhibited similar anisotropic shell growth. In the TEM images of $NaYF_4$:20% Yb^{3+}, 2% Er^{3+}@2 nm $NaYbF_4$@10 nm $NaGdF_4$ NSs in Figure S11, the CSS structure could be easily identified from the EDS results in Figure S12. Twins along the (0001) planes were formed in the $NaGdF_4$ shell due to the stress from lattice mismatch. Hence lattice mismatch is another important contributor to the anisotropic growth of a $NaREF_4$ shell.

These results suggest that anisotropic epitaxial shell growth applies to all core morphologies. Anisotropy is caused by the combination of several factors: the selective adsorption of oleic acid on specific faces of the core NCs due to the crystal structure of the latter (Figure 1e and insets in Figure 1b,d), the etching action of the oleic acid capping agent, and the lattice mismatch between core and shell components. Figure 6 shows the proposed mechanism for the epitaxial growth of $NaREF_4$ shells in UC CS NSs. The specific adsorption of oleic acid on NCs faces is the major cause of anisotropic growth. It is postulated that oleic acid adsorbed preferentially on the {0001} faces,[31,32] thereby slowing the growth in the ⟨0001⟩ direction. The evidence for this hypothesis could be drawn from previous studies: the most thermally stable morphology in a prolonged oleic acid synthesis is large flat hexagonal nanoplates.[7,33] The deposition of the $NaYbF_4$ shell in our experimental system is expected to follow the Franck-van der Merwe single layer epitaxial film growth because of the small lattice mismatch (see Table S2) between the core and shell. The faces were covered with adsorbed ligands (oleic acid) in dynamic equilibrium with the free ligands in the growth solution.[34] Oleic acid etching of the deposited shell should be quite prevalent at the high temperature used for shell growth.[35,36] The affinity of oleic acid for the {0001} faces also resulted in an accelerated etching of the {0001} faces. The competing processes of deposition and etching occurred for all thickness. In the fabrication of CS NCs with thinner shells (<2 nm), the etching action was barely compensated by the deposition of the $NaYbF_4$ shell due to the low shell precursor concentration used in the experimental system. Etching occurred on all faces especially in the ⟨0001⟩ direction. Therefore, the shell grew only noticeably on the lateral faces leaving the core {0001} faces exposed. In the case of thicker shells, etching was partially compensated by $NaYbF_4$ deposition thereby enabling some growth in the ⟨0001⟩ direction. The CS NSs in this case tend to be "fatter" than "taller". For the growth of shells with a large lattice mismatch with the core, such as $NaGdF_4$ and Eu^{3+} doped $NaGdF_4$, no growth along the *c* axis was possible. This is because, for a thin shell, while the shell would initially grow to follow the lattice of the core, ligand etching, which was greatest in the *c* direction, would negate any shell growth along the *c* axis. On the other hand, a relatively thick shell would relax into the lattice structure of $NaGdF_4$ instead of following that of the core. The strain between the mismatched core and shell was largest in the ⟨0001⟩ direction and this was relieved by sharing as few layers as possible in the *c* axis; thus, incompletely enclosed CSs were again formed.

The CS structure has been used in the UC NC design to enhance luminescence and introduce multifunctionality. It is commonly accepted that an appropriate shell would enhance the emission of the core by suppressing surface ion quenching or by harvesting more energy from the shell.[24,37,38] The effect of $NaYbF_4$

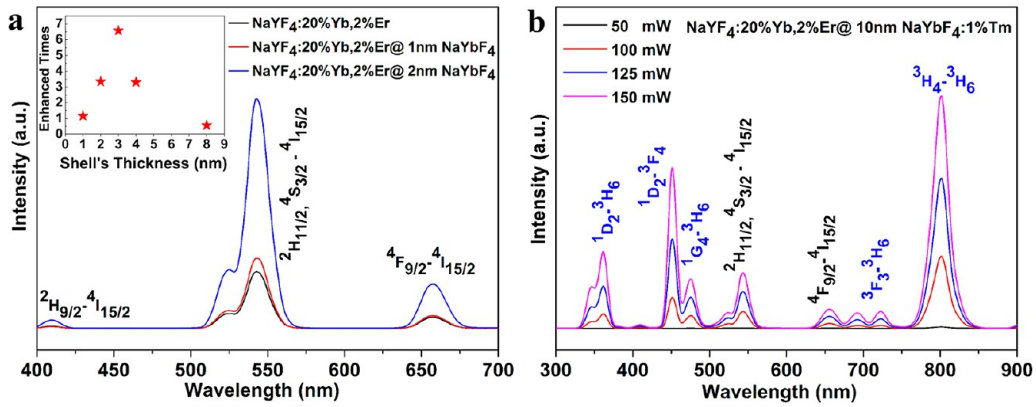

Figure 7. (a) UC luminescence spectra of $NaYF_4$:20% Yb^{3+}, 2% Er^{3+} (black) and corresponding CS NSs with 1 nm (red) and 2 nm (blue) $NaYbF_4$ shell; the inset shows the intensity ratios of the NSs relative to the core. (b) Power dependent UC emissions of $NaYF_4$:20% Yb^{3+}, 2% Er^{3+} with 10 nm $NaYbF_4$:1% Tm^{3+} shell under laser powers of 50 mW (black), 100 mW (red), 125 mW (blue), and 150 mW (magenta).

shell thickness on the emission of a $NaYF_4$:20% Yb^{3+}, 2% Er^{3+} core was therefore also investigated in this study (Figure 7a). All of the samples in this study emitted bright green emission after excitation by a 980 nm laser. The three characteristic emission bands could be indexed to the $^2H_{9/2}-^4I_{15/2}$, $^2H_{11/2}$, $^4S_{3/2}-^4I_{15/2}$, and $^4F_{9/2}-^4I_{15/2}$ transitions of Er^{3+} ions. The inset in Figure 7a shows the relation between shell thickness and emission intensity. The experimental results indicated that a thin shell (1 nm) was not effective in enhancing Er^{3+} emission. It is known that surface-related vibrations of organic species can cause the luminescence quenching of RE ions.[38] Such quenching can in theory be reduced by the deposition of a shell. Since a thin shell (*e.g.*, the 1 nm) is unlikely to provide a complete shell closure and it is also more susceptible to remnant surface defects or new defects introduced by ligand etching, the reduction in quenching-causing surface-related vibrations and surface defects was only realized with an increase in shell thickness. This, together with the effective energy transfer to Er^{3+} *via* neighboring Yb^{3+} ions in the core and the shell, yielded enhanced emission which was maximized at a thickness of ~3 nm. Above this thickness, the enhancement effect was gradually reduced. This result is significantly different from the observation of a previous study based on the $NaYF_4$:Yb,Er@$NaYF_4$ CS NS, where intensity increased monotonously with shell thickness.[38] The different shell component in our design could be the main reason. It is hypothesized that a thicker shell ($NaYbF_4$) limited the absorption of light by Yb^{3+} in the core, thereby reducing the energy transferable to Er^{3+}. Furthermore, a thicker shell also tends to grow into its own crystal habit than to follow the lattice of the core component. The strain at the interface (between the $NaYF_4$ core and $NaYbF_4$ shell) could also have impacted the core emission negatively. Therefore, enhanced emission performance was only achievable within a narrow range of shell thickness and not all CSs could deliver an enhanced performance relative to the cores. This is an important finding for understanding the shell thickness effect in enhanced emission as well as for the optimization of the CS NS design for performance enhancements.

These new findings are valuable to the design and fabrication of UC CSs. Extending the diversity of color output and introducing new functions (such as optical switching) are always the developmental goals for NSs.[1,18] Figure 7b shows the power dependent emission of $NaYF_4$:20% Yb^{3+}, 2% Er^{3+}@10 nm-thick $NaYbF_4$:1% Tm^{3+} (the cores were the 20 nm quasi-spherical NCs shown in Figure S13). NIR emissions from Tm^{3+} ($^3H_4-^3H_6$) and a weak green emission from Er^{3+} were detected at low laser powers. With the increase in laser power, both emissions from core and the shell were mutually enhanced, especially the $^1D_2-^3F_4$ and $^1G_4-^3H_6$ transitions of Tm^{3+} (shown in the plots of normalized emissions in Figure S14). The emission in the visible light region then turned to blue instead of green (see the CIE chromaticity diagram of Figure S15). Therefore, color variations were clearly a possibility with these CS NSs. More color outputs in CS NSs could then be designed based on the knowledge of anisotropic shell growth.

CONCLUSIONS

In summary, the anisotropic growth of $NaREF_4$ shell was revealed by studying a series of precision prepared CS NSs. The epitaxial growth of the shell layer was found to be faster in the lateral directions than in the ⟨0001⟩ axial direction in the oleic acid synthesis system (the most common route to preparing UC NCs). In some cases, a complete shell enclosure could not even been formed. This was most evident in CS NCs with thin shells or CS NCs with a large lattice mismatch between the core and shell components. This was caused by the strong competition between ligand etching and epitaxial shell growth, especially when the shell was thin. The lattice mismatch between the core and shell also significantly affected epitaxial shell

growth. A greater lattice mismatch would promote oblong shell growth instead of conformal surface coverage. These new findings should be highly useful for the design and precision fabrication of multifunctional UC CS NSs, and for understanding the emission mechanism in complex CS NSs.

MATERIALS AND METHODS

Materials. Yttrium oxide (Y_2O_3), ytterbium oxide (Yb_2O_3), erbium oxide (Er_2O_3), thulium oxide (Tm_2O_3), gallium oxide (Gd_2O_3), europium oxide (Eu_2O_3), trifluoroacetic acid (CF_3COOH), sodium trifluoroacetate (CF_3COONa), 1-octadecene (ODE), and oleic acid (OA) were purchased from Aldrich. Hexanes, ethanol, and methanol were purchased from Merck.

Preparation of RE $(CF_3COO)_3$ Precursor. In a typical synthesis, 0.005 mol RE_2O_3 was added to a glass bottle (volume = 15 mL) containing 2 mL of deionized water and stirred for 20 min to form a slurry. After introducing 0.033 mol CF_3COOH to the slurry, the glass bottle was sealed and stirring continued at 85 °C for 24 h, which completely turned the slurry into a clear solution. The clear filtrate obtained from filtering by a microporous membrane was heated (with stirring) at 60 °C for 24 h to evaporate excess CF_3COOH and water. The final solid products was dried under vacuum at 50 °C for another 24 h and then stored in a desiccator.

Preparation of Quasi-Spherical NCs. A total of 0.25 mmol $RE(CF_3COO)_3$ (RE = Y, Yb, Er, Tm) and 0.46 mmol $NaCF_3COO$ were introduced to a three-necked flask (25 mL) containing 4.5 mL of ODE and 1.5 mL of OA at room temperature. The mixture was stirred under vacuum for 30 min at room temperature and then slowly heated to 120 °C. It was kept at this temperature for another 20 min under vacuum and magnetic stirring to remove residual water and oxygen. The mixture was then heated to 320 °C in an Ar protecting atmosphere and kept at this temperature for 3 min and then cooled to 280 °C quickly. It was kept 280 °C for another 10 min to ripen the NCs. Thereafter, the mixture was allowed to cool to room temperature naturally. Twenty-five milliliters of absolute ethanol (or methanol) was added to precipitate the oleic acid-capped NCs. The resulting mixture was collected by centrifugation and then washed and centrifuged twice by a mixture of ethanol and hexanes. The NCs prepared as such were then dispersed in 10 mL of hexane for further use.

Preparation of Big Prisms. A total of 0.5 mmol $RE(CF_3COO)_3$ (RE = Y, Yb, Er, Tm) and 1.0 mmol $NaCF_3COO$ were introduced to a three-necked flask (25 mL) containing 3 mL of ODE and 3 mL of OA at room temperature. The mixture was stirred under vacuum for 30 min at room temperature and then slowly heated to 120 °C. It was kept at this temperature for another 20 min under vacuum and magnetic stirring to remove residual water and oxygen. The mixture was then heated to 320 °C in an Ar protecting atmosphere and kept at this temperature for 10 min and then cooled to 280 °C quickly. It was kept 280 °C for another 10 min to ripen the NCs. The following steps are the same.

Preparation of Rodlike NCs (~32 × 21 nm). A total of 0.5 mmol $RE(CF_3COO)_3$ (RE = Y, Yb, Er, Tm) and 0.88 mmol $NaCF_3COO$ were introduced to a three-necked flask (25 mL) containing 3.5 mL of ODE and 2.5 mL of OA at room temperature. The mixture was stirred under vacuum for 30 min at room temperature and then slowly heated to 120 °C. It was kept at this temperature for another 20 min under vacuum and magnetic stirring to remove residual water and oxygen. The mixture was then heated to 320 °C in an Ar protecting atmosphere and kept at this temperature for 8 min and then cooled to 280 °C quickly. It was kept 280 °C for another 10 min to ripen the NCs. The following steps are the same.

Preparation of Rodlike NCs (~43 × 27.5 nm). A total of 0.5 mmol $RE(CF_3COO)_3$ (RE = Y, Yb, Er, Tm) and 0.88 mmol $NaCF_3COO$ were introduced to a three-necked flask (25 mL) containing 3 mL of ODE and 3 mL of OA at room temperature. The mixture was stirred under vacuum for 30 min at room temperature and then slowly heated to 120 °C. It was kept at this temperature for another 20 min under vacuum and magnetic stirring to removal residual water and oxygen. The mixture was then heated to 320 °C in an Ar protecting atmosphere and kept at this temperature for 8 min and then cooled to 280 °C quickly. It was kept 280 °C for another 10 min to ripen the NCs. The following steps are the same.

Preparation of $NaREF_4$ CS NCs. In a typical synthesis, 2 mL of the core NCs solution in hexane was participated by adding ethanol followed by centrifugation at 12 000 rpm and drying at 60 °C. The collected powder was used to calculate the amount of $NaREF_4$ core (a constant of 0.9 was used; the calculated amount of cores was signed as X). For the growth of thin shells, the cores were regarded as cylinders for calculating the amount of shell precursor (Y) to use. The following formula was used, $Y/X = \{\pi(r+n)^2h - \pi r^2 h\}/\pi r^2 h$ (where n is the shell thickness, r is the NC radius, and h is the NC length). Y mmol $RE(CF_3COO)_3$ and $1.8Y$ mmol $NaCF_3COO$ were added to a 25 mL three-necked flask containing 3 mL of ODE and 3 mL of OA at room temperature. After injecting 2 mL of the core NCs solution, the mixture was stirred at 60°C for 3 h under argon protection to remove hexane from the mixture. The mixture was heated to 120 °C slowly and kept at this temperature for another 30 min under vacuum and magnetic stirring to remove residual water and oxygen. The mixture under Ar protection was then heated quickly to 280 °C and kept there for 20 min before it was allowed to cool to room temperature naturally. Twenty-five milliliters of absolute ethanol (or methanol) was added to precipitate the oleic acid capped NCs. The resulting mixture was collected by centrifugation and washed and centrifuged twice by a mixture of ethanol and hexane. The CS NSs prepared as such were then dispersed in hexane.

Characterizations. The morphology and size of the as-synthesized NSs were examined by a JEM-2100 transmission electron microscope operating at 200 kV. Energy Dispersive Spectroscopy (EDS) was recorded by an Oxford INCA attachment. The structure and the phase purity of the as-synthesized products were determined by X-ray diffraction (XRD) on a Buruker D8 diffractometer using Cu Kα radiation (λ = 1.5418 Å). X-ray photoelectron spectroscopy (XPS) spectra were performed with a Kratos AXIS Ultra^{DLD}, using a mono Al Kα X-ray source (1486.71 eV). Up-conversion luminescence was measured using a Hitachi F-500 fluorescence spectrophotometer equipped with a commercial CW IR laser (980 nm).

UC Luminescence Measurements. The recovered as-synthesized CS NCs were dispersed in 5 mL of hexane. For comparison, 2 mL of the corresponding core solution was also diluted to 5 mL. For UC detection, 3.5 mL of solution of each specimen was excited by a 100 mW, 980 nm laser.

Conflict of Interest: The authors declare no competing financial interest.

Supporting Information Available: Details of the compositions, sizes, and shell thickesses of the as-prepared CS NSs; supplementary TEM, XPS, XRD, EDS, and luminescence results. This material is available free of charge *via* the Internet at http://pubs.acs.org.

Acknowledgment. The authors would like to acknowledge Prof. Yong Zhang of Bioengineering for providing the facility and assistance in up-conversion luminescence measurements.

REFERENCES AND NOTES

1. Wang, F.; Deng, R.; Wang, J.; Wang, Q.; Han, Y.; Zhu, H.; Chen, X.; Liu, X. Tuning Upconversion through Energy Migration in Core-Shell Nanoparticles. *Nat. Mater.* **2011**, *10*, 968–973.
2. Wang, F.; Liu, X. Recent Advances in the Chemistry of Lanthanide-Doped Upconversion Nanocrystals. *Chem. Soc. Rev.* **2009**, *4*, 976–989.

3. Jayakumar, M. K. G.; Idris, N. M.; Zhang, Y. Remote Activation of Biomolecules in Deep Tissues Using Near-Infrared-to-UV Upconversion Nanotransducers. *Proc. Natl. Acad. Sci. U.S.A.* **2012**, *109*, 8483–8488.
4. Chen, F.; Bu, W.; Zhang, S.; Liu, X.; Liu, J.; Xing, H.; Xiao, Q.; Zhou, L.; Peng, W.; Wang, L.; *et al.* Positive and Negative Lattice Shielding Effects Co-existing in Gd (III) Ion Doped Bifunctional Upconversion Nanoprobes. *Adv. Funct. Mater.* **2011**, *21*, 4285–4294.
5. Zhang, F.; Braun, G. B.; Shi, Y.; Zhang, Y.; Sun, X.; Reich, N. O.; Zhao, D.; Stucky, G. Fabrication of $Ag@SiO_2@Y_2O_3$:Er Nanostructures for Bioimaging: Tuning of the Upconversion Fluorescence with Silver Nanoparticles. *J. Am. Chem. Soc.* **2010**, *132*, 2850–2851.
6. Haase, M.; Schäfer, H. Upconverting Nanoparticles. *Angew. Chem., Int. Ed.* **2011**, *50*, 5808–5829.
7. Mai, H. X.; Zhang, Y. W.; Si, R.; Yan, Z. G.; Sun, L. D.; You, L. P.; Yan, C. H. High-Quality Sodium Rare-Earth Fluoride Nanocrystals: Controlled Synthesis and Optical Properties. *J. Am. Chem. Soc.* **2006**, *128*, 6426–6436.
8. Wang, G.; Peng, Q.; Li, Y. Luminescence Tuning of Upconversion Nanocrystals. *Chem.—Eur. J.* **2010**, *16*, 4923–4931.
9. Liu, Y.; Ai, K.; Liu, J.; Yuan, Q.; He, Y.; Lu, L. High-Performance Ytterbium-Based A Nanoparticulate Contrast Agent for *in Vivo* X-Ray Computed Tomography Imaging. *Angew. Chem., Int. Ed.* **2011**, *51*, 1437–1442.
10. Liu, Q.; Sun, Y.; Yang, T.; Feng, W.; Li, C.; Li, F. Sub-10 nm Hexagonal Lanthanide-Doped $NaLuF_4$ Upconversion Nanocyrstals for Sensitive Bioimaging *in Vivo*. *J. Am. Chem. Soc.* **2011**, *133*, 17122–17125.
11. Cheng, L.; Yang, K.; Li, Y.; Chen, J.; Wang, C.; Shao, M.; Lee, S.-T.; Liu, Z. Facile Preparation of Multifunctional Upconversion Nanoprobes for Multimodal Imaging and Dual-Targeted Photothermal Therapy. *Angew. Chem., Int. Ed.* **2011**, *50*, 7385–7390.
12. Zhang, C.; Zhou, H.-P.; Liao, L.-Y.; Feng, W.; Sun, W.; Li, Z.-X.; Xu, C.-H.; Fang, C.-J.; Sun, L.-D.; Zhang, Y.-W.; *et al.* Luminescence Modulation of Ordered Upconversion Nanopatterns by a Photochromic Diarylethene: Rewritable Optical Storage with Nondestructive Readout. *Adv. Mater.* **2010**, *22*, 633–637.
13. Wang, F.; Han, Y.; Lim, C. S.; Lu, Y.; Wang, J.; Xu, J.; Chen, H.; Zhang, C.; Hong, M.; Liu, X. Simultaneous Phase and Size Control of Upconversion Nanocrystals Through Lanthanide Doping. *Nature* **2010**, *463*, 1061–1065.
14. Wang, L.; Li, P.; Li, Y. Down- and Up-Conversion Luminescent Nanorods. *Adv. Mater.* **2007**, *19*, 3304–3307.
15. Liu, Y.; Tu, D.; Zhu, H.; Li, R.; Luo, W.; Chen, X. A Strategy to Achieve Efficient Dual-Mode Luminescence of Eu^{3+} in Lanthanides Doped Multifunctional $NaGdF_4$ Nanocrystals. *Adv. Mater.* **2010**, *22*, 3266–3271.
16. Hou, Y.; Qiao, R.; Fang, F.; Wang, X.; Dong, C.; Liu, K.; Liu, C.; Liu, Z.; Lei, H.; Wang, F.; *et al.* $NaGdF_4$ Nanoparticle-Based Molecular Probes for Magnetic Resonance Imaging of Intraperitoneal Tumor Xenografts *in Vivo*. *ACS Nano* **2012**, *7*, 330–338.
17. Teng, X.; Zhu, Y.; Wei, W.; Wang, S.; Huang, J.; Naccache, R.; Hu, W.; Tok, A. I. Y.; Han, Y.; Zhang, Q.; *et al.* Lanthanide-Doped $NaxScF_{3+x}$ Nanocrystals: Crystal Structure Evolution and Multicolor Tuning. *J. Am. Chem. Soc.* **2012**, *134*, 8340–8343.
18. Boyer, J.-C.; Carling, C.-J.; Gates, B. D.; Branda, N. R. Two-Way Photoswitching Using One Type of Near-Infrared Light, Upconverting Nanoparticles, and Changing Only the Light Intensity. *J. Am. Chem. Soc.* **2010**, *132*, 15766–15772.
19. Chen, F.; Zhang, S.; Bu, W.; Chen, Y.; Xiao, Q.; Liu, J.; Xing, H.; Zhou, L.; Peng, W.; Shi, J. A Uniform Sub-50 nm-Sized Magnetic/Upconversion Fluorescent Bimodal Imaging Agent Capable of Generating Singlet Oxygen by Using a 980 nm Laser. *Chem.—Eur. J.* **2012**, *18*, 7082–7090.
20. Park, Y. I.; Kim, H. M.; Kim, J. H.; Moon, K. C.; Yoo, B.; Lee, K. T.; Lee, N.; Choi, Y.; Park, W.; Ling, D.; *et al.* Theranostic Probe Based on Lanthanide-Doped Nanoparticles for Simultaneous *in Vivo* Dual-Modal Imaging and Photodynamic Therapy. *Adv. Mater.* **2012**, *24*, 5755–5761.
21. Gai, S.; Yang, P.; Li, C.; Wang, W.; Dai, Y.; Niu, N.; Lin, J. Synthesis of Magnetic, Up-Conversion Luminescent, and Mesoporous Core-Shell-Structured Nanocomposites as Drug Carriers. *Adv. Funct. Mater.* **2010**, *20*, 1166–1172.
22. Abel, K. A.; Boyer, J.-C.; van Veggel, F. C. J. M. Hard Proof of the $NaYF_4/NaGdF_4$ Nanocrystal Core/Shell Structure. *J. Am. Chem. Soc.* **2009**, *131*, 14644–14645.
23. Wang, F.; Wang, J.; Liu, X. Direct Evidence of a Surface Quenching Effect on Size-Dependent Luminescence of Upconversion Nanoparticles. *Angew. Chem., Int. Ed.* **2010**, *49*, 7456–7460.
24. Zhang, F.; Che, R.; Li, X.; Yao, C.; Yang, J.; Shen, D.; Hu, P.; Li, W.; Zhao, D. Direct Imaging the Upconversion Nanocrystal Core/Shell Structure at the Subnanometer Level: Shell Thickness Dependence in Upconverting Optical Properties. *Nano Lett.* **2012**, *12*, 2852–2858.
25. Wang, Y.; Tu, L.; Zhao, J.; Sun, Y.; Kong, X.; Zhang, H. Upconversion luminescence of β-$NaYF_4$: Yb^{3+}, Er^{3+}@ β-$NaYF_4$ core/shell nanoparticles: excitation power density and surface dependence. *J. Phys. Chem. C* **2009**, *113*, 7164–7169.
26. Dong, C.; Korinek, A.; Blasiak, B.; Tomanek, B.; van Veggel, F. C. J. M. Cation Exchange: A Facile Method To Make $NaYF_4$:Yb,Tm-$NaGdF_4$ Core−Shell Nanoparticles with a Thin, Tunable, and Uniform Shell. *Chem. Mater.* **2012**, *24*, 1297–1305.
27. Abel, K. A.; Boyer, J.-C.; Andrei, C. M.; van Veggel, F. C. J. M. Analysis of the Shell Thickness Distribution on $NaYF_4$/ $NaGdF_4$ Core/Shell Nanocrystals by EELS and EDS. *J. Phys. Chem. Lett.* **2011**, *2*, 185–189.
28. Su, Q.; Han, S.; Xie, X.; Zhu, H.; Chen, H.; Chen, C.-K.; Liu, R.-S.; Chen, X.; Wang, F.; Liu, X. The Effect of Surface Coating on Energy Migration-Mediated Upconversion. *J. Am. Chem. Soc.* **2012**, *134*, 20849–20857.
29. Manna, L.; Scher, E. C.; Li, L. S.; Alivisatos, A. P. Epitaxial Growth and Photochemical Annealing of Graded CdS/ZnS Shells on Colloidal CdSe Nanorods. *J. Am. Chem. Soc.* **2002**, *124*, 7136–7145.
30. Zhang, F.; Wan, Y.; Shi, Y.; Tu, B.; Zhao, D. Ordered Mesostructured Rare-Earth Fluoride Nanowire Arrays with Upconversion Fluorescence. *Chem. Mater.* **2008**, *20*, 3778–3784.
31. Zhao, J.; Sun, Y.; Kong, X.; Tian, L.; Wang, Y.; Tu, L.; Zhao, J.; Zhang, H. Controlled Synthesis, Formation Mechanism, and Great Enhancement of Red Upconversion Luminescence of $NaYF_4$:Yb^{3+}, Er^{3+} Nanocrystals/Submicroplates at Low Doping Level. *J. Phys. Chem. B* **2008**, *112*, 15666–15672.
32. Zhang, F.; Wan, Y.; Yu, T.; Zhang, F.; Shi, Y.; Xie, S.; Li, Y.; Xu, L.; Tu, B.; Zhao, D. Uniform Nanostructured Arrays of Sodium Rare-Earth Fluorides for Highly Efficient Multicolor Upconversion Luminescence. *Angew. Chem., Int. Ed.* **2007**, *46*, 7976–7979.
33. Ye, X.; Collins, J. E.; Kang, Y.; Chen, J.; Chen, D. T. N.; Yodh, A. G.; Murray, C. B. Morphologically Controlled Synthesis of Colloidal Upconversion Nanophosphors and Their Shape-Directed Self-Assembly. *Proc. Natl. Acad. Sci. U.S.A.* **2010**, *107*, 22430–22435.
34. Pradhan, N.; Reifsnyder, D.; Xie, R.; Aldana, J.; Peng, X. Surface Ligand Dynamics in Growth of Nanocrystals. *J. Am. Chem. Soc.* **2007**, *129*, 9500–9509.
35. Mulvihill, M. J.; Ling, X. Y.; Henzie, J.; Yang, P. Anisotropic Etching of Silver Nanoparticles for Plasmonic Structures Capable of Single-Particle SERS. *J. Am. Chem. Soc.* **2009**, *132*, 268–274.
36. Wu, H.; Chen, O.; Zhuang, J.; Lynch, J.; LaMontagne, D.; Nagaoka, Y.; Cao, Y. C. Formation of Heterodimer Nanocrystals: UO_2/In_2O_3 and $FePt/In_2O_3$. *J. Am. Chem. Soc.* **2011**, *133*, 14327–14337.
37. Fiorenzo, V.; Rafik, N.; Venkataramanan, M.; Christopher, G. M.; John, A. C. The Active-Core/Active-Shell Approach: A Strategy To Enhance the Upconversion Luminescence in

Lanthanide-Doped Nanoparticles. *Adv. Funct. Mater.* **2009**, *19*, 2924–2929.
38. Wang, Y.; Liu, K.; Liu, X.; Dohnalová, K.; Gregorkiewicz, T.; Kong, X.; Aalders, M. C. G.; Buma, W. J.; Zhang, H. Critical Shell Thickness of Core/Shell Upconversion Luminescence Nanoplatform for FRET Application. *J. Phys. Chem. Lett.* **2011**, *2*, 2083–2088.